Analysis of Water in Confined Geometries and at Interfaces

Michael D. Fayer[1] and Nancy E. Levinger[2]

[1]Department of Chemistry, Stanford University, Stanford, California 94305; email: fayer@stanford.edu

[2]Department of Chemistry, Colorado State University, Fort Collins, Colorado 80523; email: levinger@lamar.colostate.edu

Annu. Rev. Anal. Chem. 2010. 3:89–107

First published online as a Review in Advance on February 19, 2010

The *Annual Review of Analytical Chemistry* is online at anchem.annualreviews.org

This article's doi: 10.1146/annurev-anchem-070109-103410

1936-1327/10/0719-0089$20.00

Key Words

ultrafast infrared pump-probe spectroscopy, reverse micelles, nanoscopically confined water, hydrogen bond dynamics, orientational dynamics

Abstract

The properties of water depend on its extended hydrogen bond network and the continual picosecond–time scale structural evolution of the network. Water molecules in confined environments with pools a few nanometers in diameter or at interfaces undergo hydrogen bond structural dynamics that differ drastically from the dynamics they undergo in bulk water. Orientational motions of water require hydrogen bond network rearrangement. Therefore, observations of orientational relaxation in nanoscopic water systems provide information about the influence of confinement and interfaces on hydrogen bond dynamics. Ultrafast infrared polarization- and wavelength-selective pump-probe experiments can measure the orientational relaxation of water and distinguish water at an interface from water removed from an interface. These experiments can be applied to water in reverse micelles (spherical nanopools). The results provide quantitative determination of the dynamics of water as a function of the size and nature of the confining structure.

1. INTRODUCTION

Water exists in confined environments and at interfaces in a wide variety of important systems in chemistry, biology, geology, materials science, and technological applications. In biology, water is found in crowded environments such as cells, in which it hydrates membranes and large biomolecules, as well as pockets in proteins. In geology, interfacial water molecules can control ion adsorption and mineral dissolution. Embedded water molecules can change the structure of zeolites. In chemistry, water plays an important role as a polar solvent that is often in contact with interfaces, for example, in ion-exchange resin systems and chromatographic surfaces. Water in the nanoscopic channels of polyelectrolyte membranes is central to the operation of hydrogen fuel cells.

Water's unique properties can be traced to its formation of an extended hydrogen bonding network (1). Water molecules can form up to four hydrogen bonds in an approximately tetrahedral arrangement (2). Water is a very small molecule; in the absence of hydrogen bonds it would be a gas at room temperature, as is methane, which is very similar in size and molecular weight. The hydrogen bonds give water its stability as a room-temperature liquid. However, the hydrogen bonded network is not static. The network evolves constantly on a picosecond time scale because of the concerted dissociation and formation of hydrogen bonds (3, 4). This rapid evolution of water's hydrogen network enables processes ranging from proton diffusion to protein folding.

Recent advances in both experiments and theory have greatly increased our understanding of dynamics of water in bulk solution (4–14). Ultrafast infrared (IR) vibrational echo experiments have measured spectral diffusion in bulk water (15–24). The results have been compared to detailed simulations (17, 19, 25–28). Experiments and simulations show that on very short (<400-fs) time scales, local fluctuations in hydrogen bond lengths and angles dominate the hydrogen bond dynamics. At longer (>1-ps) time scales, the hydrogen bond network evolution randomizes the water network structure. Ultrafast IR polarization-selective pump-probe experiments have been used to measure orientational relaxation in bulk water (6, 13, 21, 29–33). Following an ultrafast inertial component (6) occurring on a time scale of ~100 fs, bulk water undergoes complete orientational relaxation by jump reorientation (3, 4, 6, 34). This concerted process involves a water molecule and its first two "solvation shells" of other water molecules. Water molecules undergo orientational relaxation by breaking and reforming hydrogen bonds with new partners. In bulk water, they do so by making ~60° jumps.

Experiments on bulk water generally measure the dynamics of HOD in either H_2O or D_2O (1, 17, 18, 33, 35). For example, the OD stretching mode of dilute HOD in H_2O allows measurements to eliminate the vibrational excitation transport that contributes to spectral diffusion and anisotropy decay in pure H_2O and D_2O (36, 37). Simulations have shown that the presence of dilute HOD does not change the dynamics of H_2O; the dynamics reported by dilute HOD in H_2O are a good representation of the dynamics in pure H_2O. (25). Measurements of the OD orientational relaxation decay time of HOD in H_2O reveal a 2.6-ps single exponential decay after the initial inertial relaxation (6). Similarly, the OH orientational relaxation of HOD in D_2O is reported as 2.5 ps (33).

Here we discuss recent experiments on the influence of nanoscopic confinement and interfaces on water hydrogen bond dynamics (38–45). Water is confined to the interior of reverse micelles, which are droplets of water sequestered from a nonpolar phase by a surfactant layer (46). In the studies described below, the surfactant Aerosol OT [AOT; sodium bis(2-ethylhexyl) sulfosuccinate] forms well-defined reverse micellar structures whose centers contain a nanoscopic pool of water. **Figure 1** shows the chemical structure of AOT and an illustration of an AOT reverse micelle. The reverse micelles are in an organic phase, in this case iso-octane. The negatively charged

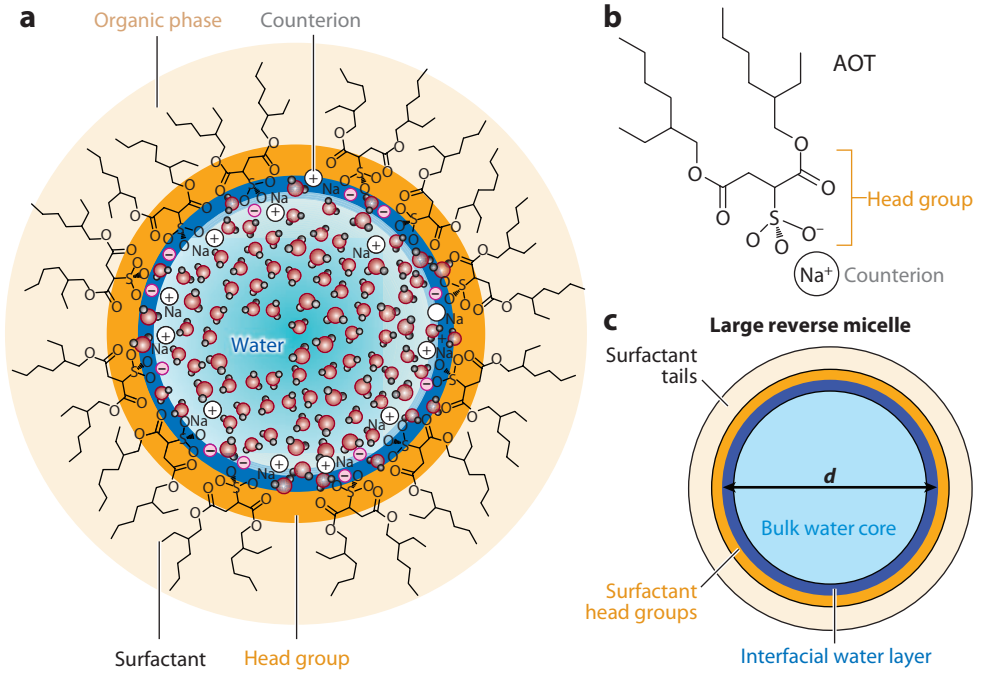

Figure 1

(*a*) Schematic depiction of a potential structure of a reverse micelle. Water molecules reside in the interior, sometimes interacting with head groups and counterions. Surfactant tails reside in contact with the continuous, nonpolar, organic supporting phase. (*b*) Chemical structure of Aerosol OT [AOT; sodium bis(2-ethylhexyl) sulfosuccinate], the surfactant used in the studies reported in this review. (*c*) Schematic of a large reverse micelle showing important features of the structure.

sulfonate head groups with their positively charged sodium counterions form the interface between the surfactant and the nanoscopic pool of water. The counterions are in close proximity to the sulfonate anions (47).

The size of the water pool depends on the molar ratio of water to surfactant, $w_0 = [H_2O]/[AOT]$, which can be varied over a wide range of diameters, d (46, 48). Such variation makes it possible to determine the influence of the size of a water nanopool on water dynamics and, for large reverse micelles, to determine the distinct dynamics at the interface. AOT forms well-characterized, nominally monodispersed, spherical reverse micelles in iso-octane over a large range of water content from $w_0 \approx 0$ (low; essentially dry) to $w_0 \approx 60$ (high) (48). The smallest reverse micelles (50–100 water molecules) have radii of <1 nm, whereas the largest (~400,000 water molecules) have radii of up to 14 nm. This large size range allows one to change the relative amount of the water directly interacting with the interface from a large fraction to a small fraction of the total simply by increasing w_0. Here, we report on studies exploring the nature of water in a range of reverse micelle sizes: $w_0 = 2$, 5, 10, 16.5, 25, 37, and 46. Sizes for these reverse micelles, determined by photon correlation spectroscopy (48) and viscosity measurements (49), are reported to have diameters of 1.6, 2.3, 4, 5.8, 9, 17, and 20 nm, respectively.

In very large reverse micelles ($w_0 > 30$, $d \approx 10$ nm), many aspects of water exhibit properties similar to those of a bulk-like water core and water at an interface (9, 43, 50–53). Water at the interface undergoes orientational relaxation that is substantially slower than that of bulk water (9, 43, 50–53). Furthermore, water at the interface of large AOT reverse micelles has the same

orientational relaxation time as water at the interface of the planar lamellar structures (52). For very small reverse micelles ($d \approx 2.5$ nm), there are so few water molecules that all of the water is substantially affected by interactions with the interface. There is no bulk-like core, and within experimental error, orientational relaxation is slow and identical for all of the water molecules (9, 43, 53). Intermediate-size water nanopools ($d \approx 4$ nm) include both core and interfacial water molecules with distinct dynamics. However, the core exhibits dynamics that are slower than those of bulk water, and the interfacial water dynamics are slower than those at the interface of large reverse micelles. These experimental results show that the dynamics are very sensitive to the size of the confining structure for intermediate and small sizes. However, certain systems, namely those that are large enough that water in an interfacial layer interacts with so much water that it is effectively bulk water, display no size dependence.

2. TECHNICAL DETAILS OF EXPERIMENTAL STUDIES

The setup of experiments on water in confined geometries and at interfaces has been described in other publications (1, 9, 40, 42, 43, 45, 50–54). However, we provide some details of these experiments to inform the reader of the methods used. Experiments explored the OD stretch of dilute HOD in H_2O to eliminate complications due to vibrational excitation transfer that can cause artificial decay of the orientational correlation function (55, 56). Molecular dynamics (MD) simulations of HOD in bulk H_2O demonstrate that dilute HOD does not change the properties of water, and the dynamics of HOD report on the dynamics of water (19).

Time-dependent signals resolve the relative polarization of pump and probe beams collecting data for probes that are parallel ($I_\parallel$) and perpendicular ($I_\perp$) to the pump beam. These signals contain information about both the population relaxation and the orientational dynamics of the HOD molecules, given by (57)

$$I_\parallel = P(t)[1 + 0.8C_2(t)] \quad \text{and} \tag{1}$$

$$I_\perp = P(t)[1 - 0.4C_2(t)], \tag{2}$$

where $P(t)$ is the vibrational population relaxation and $C_2(t)$ is the second Legendre polynomial orientational correlation function. Pure population relaxation can be extracted from $I_\parallel$ and $I_\perp$ from Equation 3:

$$P(t) = I_\parallel + 2I_\perp. \tag{3}$$

In the case of a single ensemble of molecules undergoing orientational relaxation, the orientational correlation function, $C_2(t)$, can be determined from the anisotropy, $r(t)$, by

$$r(t) = (I_\parallel - I_\perp)/(I_\parallel + 2I_\perp) = 0.4C_2(t). \tag{4}$$

The additional complications that arise in calculating the anisotropy when there are two distinct subensembles of molecules in the system are discussed in detail below. For bulk water, the OD stretch of dilute HOD in H_2O has a vibrational population relaxation time of 1.8 ps, and the orientational relaxation time is 2.6 ps (43).

The responses from water in reverse micelles fall into several separate regimes according to the size of the water pool. We discuss results for large-, small-, and intermediate-size reverse micelles in the following three sections.

3. WATER IN LARGE REVERSE MICELLES

In all reverse micelles, some water molecules reside in the interfacial layer near surfactant head groups (46). **Figure 1*c*** depicts a large reverse micelle, showing the interfacial water layer and

the core that constitute the water pool with diameter d. For a sufficiently large micelle, much of the water resides so far from the interface that the core appears to adopt bulk-like properties, as discussed in detail below. Despite the large volume of water in the core that is bulk-like, our ultrafast IR pump-probe experiments can determine the dynamics of the interfacial layer.

The IR spectra of the OD stretch of dilute HOD in H_2O of several large reverse micelles ($w_0 = 46$, 37, 25), bulk water, and the $w_0 = 2$ reverse micelle are shown in **Figure 2*a***. Even though the OD stretch spectrum from the large reverse micelles closely resembles the signal from bulk water, OD moieties interacting with the interface contribute to the signal. This contribution manifests itself by a minuscule blueshift in the absorption spectra. As the reverse micelle size decreases, the blueshift becomes more apparent. For the tiny $w_0 = 2$ reverse micelle sample, the OD stretch displays a dramatic shift away from the signal in bulk water, and the absorption

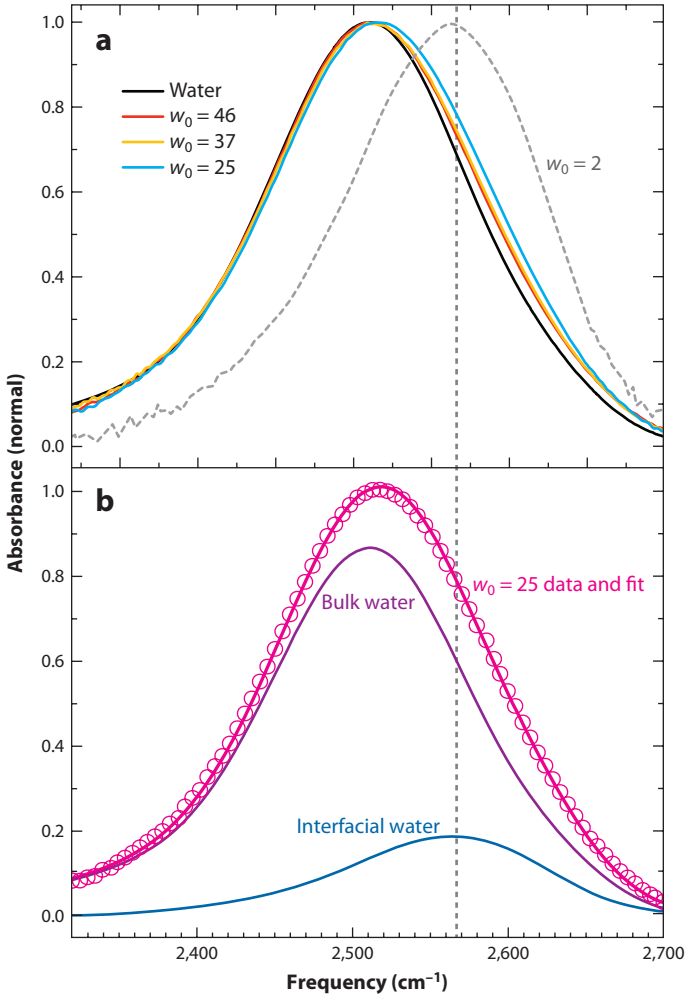

Figure 2

(*a*) Infrared (IR) spectra of the OD stretch of 5 mol% HOD in H_2O in several large ($w_0 = 46$, 37, and 25) reverse micelles, in small ($w_0 = 2$) reverse micelles, and in bulk water. (*b*) Fit of the OD stretch moiety in the IR spectrum of the $w_0 = 25$ reverse micelle via a linear combination of the bulk water spectrum and the $w_0 = 2$ spectrum. The $w_0 = 2$ spectrum represents water dominated by an interfacial environment.

spectrum peaks at ~2565 cm^{-1}. The blueshifting of the absorption spectrum with decreasing w_0 demonstrates that when water molecules interact with the interface, their OD stretching frequencies increase. As the size of the reverse micelle decreases, greater numbers of the water molecules interact with the interface, giving rise to the increased blueshift.

We have used a core/shell model to describe the water inside large reverse micelles (43). This model utilizes the spectrum of bulk water to represent the core spectrum, whereas the shell (interfacial) spectrum is modeled as the spectrum of the $w_0 = 2$ reverse micelle. In large reverse micelles, the spectrum of bulk water represents the core spectrum very well. We use the OD spectrum in $w_0 = 2$ reverse micelles to represent interfacial water because, in this tiny reverse micelle, essentially all of the water molecules interact directly with the interface. Therefore, the $w_0 = 2$ spectrum acts as a useful guide to help identify the probably spectral region of interfacial water.

Figure 2*b* shows the results of a fit to the spectrum of a $w_0 = 25$ reverse micelle. The fit was made with a linear combination of the bulk water spectrum and the $w_0 = 2$ spectrum, where the relative amplitude of the two spectra is the only adjustable parameter. The fit is very good. Clearly, the response from interfacial water contributes more strongly to the pump-probe signal at frequencies higher than 2565 cm^{-1}. However, even on the blue (high-frequency) side of the absorption spectrum, contributions from the core bulk water and the interfacial spectra overlap extensively, demonstrating that we must separate these contributions when analyzing the time-dependent experiments.

As mentioned above, although measurements on bulk water reveal a single-exponential population relaxation (1.8 ps), and although after the ultrafast inertial component the orientational anisotropy decay is also single exponential (2.6 ps) (1), the population and orientational relaxations of OD in reverse micelle samples do not fit to single-exponential decays (6, 9, 43, 52, 53). A two-component model allows us to separate the contributions from the core bulk water and the interfacial shell water in the population decays and orientational (anisotropy) decays. We know that the core bulk water signals decay single exponentially, and we assume that the interfacial water population and anisotropy decays are also single exponential. Equations 1 and 2 above present formulas reflecting contributions to the pump-probe signal with the probe resolved parallel and perpendicular to the pump. When there is more than one subensemble in a system, and when exchange between the ensembles is slow, the contributions of each subensemble to the signal are additive, and a weighted sum of the population relaxation of the two components can describe the population relaxation:

$$P(t) = a\,P_1(t) + (1-a)P_2(t) = a\,e^{-t/T_1^w} + (1-a)e^{-t/T_1^i}. \quad (5)$$

Here, a is a weighting factor and $P_j(t)$ is the population relaxation of component j. T_1^w is the OD stretch vibrational lifetime of bulk water, and T_1^i is the lifetime of interfacial water. Importantly, because the pump-probe signal for each component is proportional to $\mu_j^4 c_j$, where μ_j is the transition dipole moment and c_j is the concentration of component j, the weighting factor a depends on both the transition dipole moment and the concentration. If the transition dipole moments of the two subensembles are the same, then a is the fractional concentration of the two species at a particular wavelength. It is not necessary to know the relative transition dipole moments of the ensembles to fit the data, and in the discussion below, a is treated as a weighting factor. However, at the same detection wavelength, the transition dipoles of the core and interfacial water are the same within experimental error (53).

Although the population relaxation behaves in an intuitive manner when more than one subensemble is present, the anisotropy decay becomes quite complicated. The additive model with contributions from interfacial and core (bulk-like) water can be expanded from the

expression in Equation 4 to

$$r(t) = \frac{a\left(I_{\parallel}^{1} - I_{\perp}^{1}\right) + (1-a)\left(I_{\parallel}^{2} - I_{\perp}^{2}\right)}{a\left(I_{\parallel}^{1} + 2I_{\perp}^{1}\right) + (1-a)\left(I_{\parallel}^{2} + 2I_{\perp}^{2}\right)} = 0.4\frac{a e^{-t/T_1^w} e^{-t/\tau_r^w} + (1-a)\, e^{-t/T_1^i} e^{-t/\tau_r^i}}{a e^{-t/T_1^w} + (1-a) e^{-t/T_1^i}}. \quad (6)$$

Here, the parallel and perpendicular pump-probe signals arising from component j are given by $I_{\parallel}^{j}$ and $I_{\perp}^{j}$, respectively. On the right-hand side of Equation 6, the single-exponential population decays and the orientational relaxation decays explicitly substitute for $I_{\parallel}^{j}(t)$, and $I_{\perp}^{j}$. τ_r^w and τ_r^i are the orientational relaxation times for bulk water and interfacial water, respectively. In the limit of a single component, the population relaxation divides out of the right-hand side of Equation 6. With multiple components, the anisotropy decay is not simply a measurement of the orientational correlation function. If the two components have a large separation of time scales for both their vibrational lifetimes and their orientational dynamics, then when the fast component has decayed away, the long-time anisotropy decay accurately represents the anisotropy of the slow component. However, at intermediate times, the anisotropy decay does not necessarily behave in an intuitive fashion, and Equation 6 is required to extract the orientational dynamics. As discussed in detail elsewhere (43), exchange of water molecules between the interfacial region and the core is slow compared to the population and orientational relaxation dynamics. Therefore, the two-component model embodied in Equations 5 and 6 is appropriate for the data analysis.

Figure 3 shows a series of simulated anisotropy decay curves with all parameters fixed except for the weighting term, a. The parameters were chosen to be representative of bulk water and interfacial water. The vibrational lifetime and orientational relaxation time of the core component were set to the bulk water values, $T_1^w = 1.8$ ps and $\tau_r^w = 2.6$ ps. The vibrational lifetime and orientational time of the interfacial component were set at $T_1^i = 4.5$ ps and $\tau_r^i = 20$ ps, which are similar to the values determined experimentally (see below). **Figure 3** clearly shows that at long times the curves coalesce to a single decay, demonstrating that after the fast vibrational

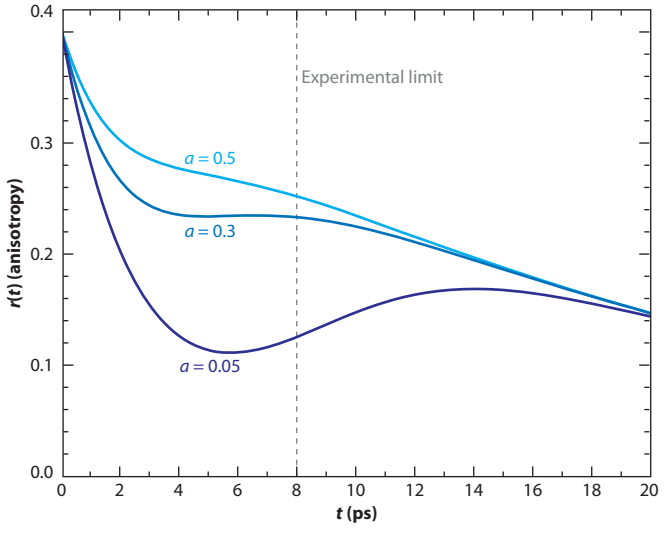

Figure 3

Simulated anisotropy decay curves depicting a two-component system decaying according to Equation 6. The parameters corresponding to population and orientational relaxation for bulk and interfacial water are fixed. Only the relative fraction of bulk water weighting term, a, varies. The vertical dashed line indicates the experimental limit imposed by the vibrational lifetimes, beyond which we cannot measure the anisotropy.

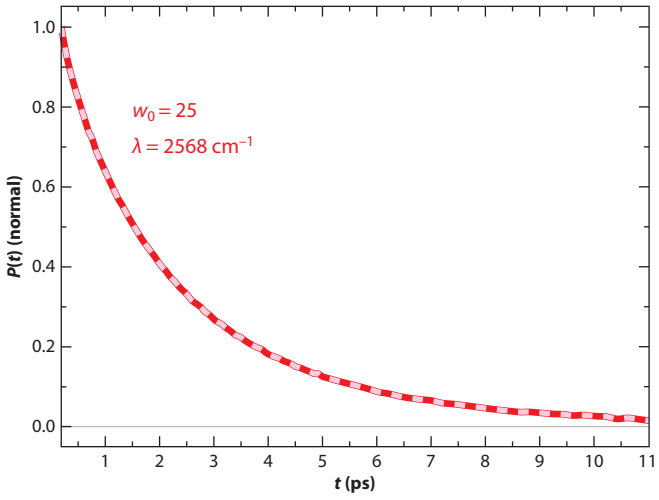

Figure 4

Population relaxation data for water in $w_0 = 25$ reverse micelles observed at 2568 cm^{-1} (*red curve*) and a biexponential fit to the data according to Equation 5 (*pink dashed curve*).

lifetime component decays, the anisotropy decay represents the orientational dynamics of the slow component. However, at intermediate times, the anisotropy can behave in a complex manner, appearing to reach a plateau value for $a = 0.3$ and even turning up for $a = 0.05$. Because they are shorter than the orientational decays, the vibrational lifetimes limit the experimental data collection, precluding observation of the complete anisotropy decay. Nonetheless, the shape of the curve out to the experimental limit is very sensitive to the decay parameters, allowing one to extract the interfacial orientational relaxation times (9).

We have studied a range of large reverse micelles with $w_0 = 16.5$, 25, 37, and 46 [5.8-, 9-, 17-, and 20-nm diameters, respectively (48, 49)]. **Figure 4** shows the population relaxation data for $w_0 = 25$ observed at 2568 cm^{-1}, which is near the peak of the spectrum of the interfacial ODs, along with a biexponential fit to the data according to Equation 5. In the fit, the bulk water lifetime was fixed with $T_1^w = 1.8$ ps. This excellent fit yields $T_1^i = 4.3 \pm 0.5$ ps for the lifetime of the OD stretch at the interface. Population decays measured at a number of frequencies for each sample revealed that within experimental error, the population decay times were independent of frequency. Changing the frequency altered only the weighting parameter a (see Equation 5) because the relative contribution from the bulk-like core water and the interfacial water varied (see **Figure 2**). We found that the vibrational lifetimes for water at the interface of the large reverse micelles with $w_0 = 16.5$, 25, 37, and 46 were 4.4 ps, 4.3 ps, 4.6 ps, and 3.9 ps, respectively, all with error bars of ± 0.5. Because these values are the same within experimental error, we used an interfacial lifetime of 4.3 ps in the analysis of the orientational relaxation time for all of the large reverse micelles.

Figure 5 compares the anisotropy decay for $w_0 = 25$ at 2568 cm^{-1} and the bulk water decay. The data are shown beginning at ~200 fs, reflecting decays obtained after the ultrafast inertial decay is complete (53) and resulting in a starting value of less than 0.4 for the long-time anisotropy decay (58). We used Equation 6 to fit the reverse micelle data but with a $t = 0$ value (rather than a $t = 0.4$ value) from the experimental data, omitting the inertial component. We knew all of the parameters for Equation 6 except for the interfacial orientation relaxation time, τ_r^i. We used values from the bulk water for the core water: $T_1^w = 1.8$ ps and $\tau_r^w = 2.6$ ps. The interfacial population

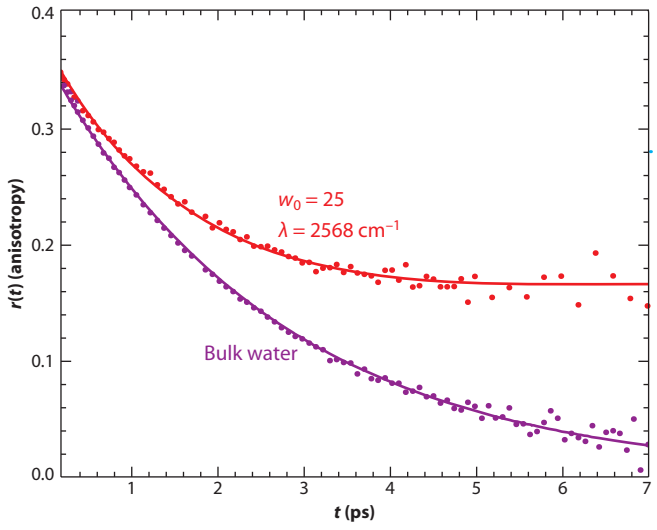

Figure 5

Anisotropy decay for water (5% HOD in H_2O) in $w_0 = 25$ reverse micelles at 2568 cm^{-1}. Also shown for the sake of comparison is the bulk water decay. Circles represent the data. The solid purple curve through the bulk water decay is a single exponential fit that yields an orientational relaxation time of 2.6 ps. The red line is a fit to the $w_0 = 25$ according to Equation 6. Displaying data after the sub-200-fs inertial decay causes the long-time anisotropy data to begin at a value below 0.4.

relaxation time was determined by fits such as that shown in **Figure 4**, for instance, $T_1^i = 4.3$ ps. Fits to population relaxation at each wavelength determined the *a* value. Simultaneously fitting data at a variety of wavelengths yielded fits such as that shown in **Figure 5**. Use of the same fitting procedure for all of the large reverse micelles yielded $\tau_r^w = 17$ ps, 19 ps, 18 ps, and 18 ps for $w_0 = 16.5$, 25, 37, and 46, respectively. For all of the samples, we estimated error bars of ± 3 ps on the basis of all of the parameters and assumptions used in the fits, rather than on the basis of the reproducibility of the data. Within experimental error, the orientational relaxation times for water molecules at the interfaces of large AOT reverse micelles were identical: $\tau_r^w = 18 \pm 3$ ps.

The important result from these studies is that the orientational relaxation time of water interacting with the AOT interface in large reverse micelles is 18 ps, and this value is independent of the size of the large reverse micelles. Experiments on AOT lamellar structures, which have planar slabs of water, found the same orientational relaxation time for water at the AOT interface (52). Recent experiments on nonionic reverse micelles demonstrate that the nature of the interface (ionic versus nonionic) has only a small effect on the interfacial orientational relaxation time (51). The slower orientational relaxation—18 ps for interfacial water compared to 2.6 ps for bulk water—is caused principally by the presence of the interface rather than by its specific chemical composition. A recently developed theory of water jump reorientation for water surrounding a hydrophobic solute proposes an explanation (3, 8). Water orientational relaxation is a concerted process involving many water molecules. For orientational relaxation to occur, a water molecule in the second solvation shell must move into the first solvation shell. One of the water molecules in the first solvation shell, which is hydrogen bonded to the so-called central water molecule of interest, breaks its hydrogen bond and forms a new hydrogen bond with another water molecule. The water that moved in from the second solvation shell reforms a hydrogen bond with the central water. At an interface, many of the paths for hydrogen bond dissociation and formation are blocked, greatly impeding the process. It is the interface that blocks hydrogen bond switching

paths, rather than the interactions with specific chemical species such as the AOT sulfonate group, that dictates the water orientational relaxation time for molecules at interfaces (45).

For large reverse micelles, comparing the contributions to the signal from interfacial water molecules in both the IR spectra and the pump-probe spectra indicates that the transition dipole moments of these two species are very similar at the same frequency. This similarity allows the fractional concentration of interfacial water to be determined from the integrated area of the interfacial water spectrum (modeled as the $w_0 = 2$ spectrum) and the a parameters to be obtained from fits to the time-dependent data (9). On the basis of geometric criteria, the data demonstrate that the most strongly perturbed interfacial water lies in the first hydration layer at the surface.

4. WATER IN SMALL REVERSE MICELLES

Although large reverse micelles have diameters large enough that water in the core region of water pools far removed from the interface has properties similar to those of bulk water, small reverse micelles behave dramatically differently. Large reverse micelles behave like systems (*a*) that contain interfacial water, (*b*) whose dynamics differ dramatically from those of bulk water, and (*c*) that contain an effectively infinite volume of bulk-like water. That the nature of the water at the interface of large reverse micelles and the water at the interface of lamellar structures are identical reinforces this idea (52, 53). Small reverse micelles have so little water that the influence of the interface permeates the entire water nanopool, and none of this water has the properties of bulk water.

Figure 6 displays anisotropy decays for water (HOD in H_2O) for $w_0 = 2$ at two wavelengths, as well as a decay in bulk water for comparison (9). Decays in small reverse micelles were measured over a range of wavelengths on the blue side of the spectrum. Following the inertial component, the data show a very fast decay followed by a very slow decay. The very fast decay (~500 fs) is

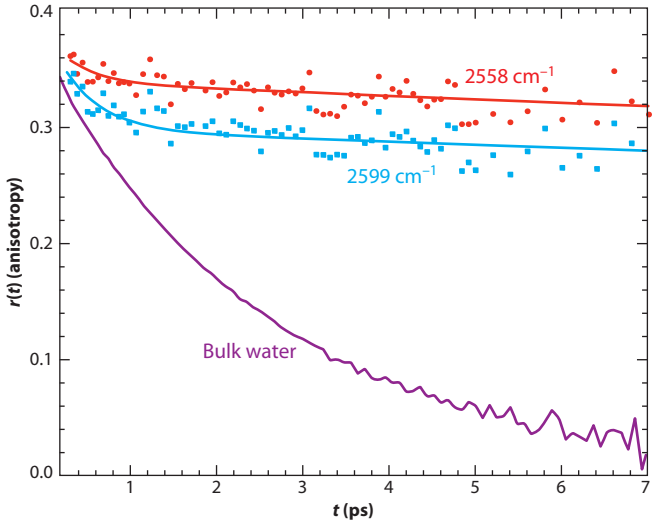

Figure 6

Anisotropy decays for water (5% HOD in H_2O) in $w_0 = 2$ Aerosol OT [sodium bis(2-ethylhexyl) sulfosuccinate] reverse micelles at 2558 cm^{-1} (*red circles*) and 2599 cm^{-1} (*blue squares*). Also shown is a decay in bulk water (*purple line*) for comparison. Reverse micelle data are fit to a wobbling-in-a-cone model (*red and blue lines through points*). Displaying data after the sub-200-fs inertial decay causes the long-time anisotropy data to begin at a value less than 0.4.

much faster than the bulk water decay (2.6 ps). Such decays have previously been observed in a number of systems (43, 50, 59, 60). The very fast decay is not a separate ensemble undergoing orientational relaxation that is much faster than that in bulk water; rather, it arises from what is referred to as wobbling in a cone (50). On a time scale that is short compared to that of complete orientational relaxation—which for small reverse micelles is very long—the OD transition dipole, which is essentially along the OD bond vector, can sample a restricted cone of angles without breaking hydrogen bonds. The hydrogen bond network is not rigid and therefore permits angular fluctuation of the intact hydrogen bond network. This wobbling motion is responsible for the fast decay component shown in **Figure 6**.

The long-time portions of the $w_0 = 2$ anisotropy decays shown in **Figure 6** and those at additional wavelengths (not shown) display the same decay, independent of wavelength, within experimental error. The lack of a wavelength dependence and the assignment of the very fast initial decay to the wobbling motions indicate that the $w_0 = 2$ reverse micelles do not contain distinct core and interfacial water components. Nearly identical behavior has been observed for $w_0 = 5$ decays (**Figure 7**), except the slow component decays substantially faster than in $w_0 = 2$. The slow components of the anisotropy decays are 110 ± 40 ps and 30 ± 3 ps for $w_0 = 2$ and $w_0 = 5$, respectively. The large error bars for the $w_0 = 2$ data arise from the difficulty of determining such a slow decay from the limited time range of the data. However, over this limited time range the decay is very well approximated as linear, so it is necessary only to determine the slope of the fit line.

The data show that, within experimental error, the orientational relaxation of water in small reverse micelles behaves as though there were a single ensemble rather than a core and an interfacial region. As mentioned above, the jump-reorientation model for bulk water demonstrates that the first and second solvation shells are involved in orientational relaxation (3, 4). For a reverse micelle to have a bulk-like core, there must be a significant number of water molecules far enough removed from the interface that the interface perturbs neither these molecules nor their first and second

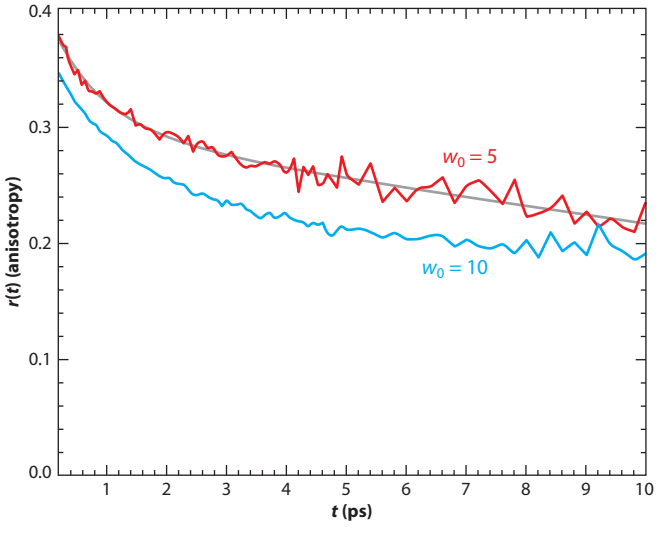

Figure 7

Anisotropy decays for water (5% HOD in H_2O) in $w_0 = 5$ (*red line*) and $w_0 = 10$ (*blue line*) reverse micelles at 2558 cm^{-1}. The data are fit to a biexponential decay (*gray line*). Displaying data after the sub-200-fs inertial decay causes the long-time anisotropy data to begin at a value less than 0.4.

solvation shells (9). For AOT reverse micelles with $w_0 = 2$, no water molecules meet this criterion. For $w_0 = 5$, and for reverse micelles for which w_0 is somewhat bigger than 5 (see Section 5), almost no water molecules meet this condition. Therefore, the water molecules do not divide into two subensembles of core and interfacial water. The effect of the interface strongly perturbs all of the water molecules in the nanopool. The long-time decay for $w_0 = 5$ is substantially faster than that for $w_0 = 2$ because there are more water molecules that are not in direct contact with the interface. This situation allows for more facile concerted hydrogen bond rearrangement and therefore faster orientational relaxation.

The results for water in small reverse micelles differ from the results for water in large reverse micelles. Anisotropy decays for intramicellar water in large micelles are nonexponential and fit well to the two-component model, in which one of the components has the bulk water lifetime and orientational relaxation time. Although the decays for large reverse micelles appear to depend on the detection frequency, we have shown that this dependence is caused by the change in value of the relative amplitude parameter a (see Equations 5 and 6). Depending on the wavelength, the interfacial water makes a larger or smaller contribution to the signal. The lifetimes and the orientational relaxation times are independent of wavelength, within experimental error, but the amount of each component changes with wavelength. In contrast, essentially all the water molecules in small reverse micelles interact with the reverse micellar interface. Their dynamics reflect the disruption of a regular hydrogen bonding network with nearby water molecules.

5. INTERMEDIATE-SIZE REVERSE MICELLES

Between large ($w_0 \geq 16.5$) reverse micelles and small ($w_0 \leq 5$) reverse micelles lies a transitional region centered about $w_0 = 10$. For $w_0 \geq 16.5$, a two-ensemble behavior with a bulk-like water core and interfacial water explains the data well. The water dynamics in the core and at the interface for large reverse micelles are independent of the water nanopool size and of frequency. For $w_0 \leq 5$, the presence of the interface strongly influences all of the water molecules, and there is no clear separation into core and interfacial regions. In the intermediate region, the dynamics in reverse micelles depend strongly on the size of the water nanopool.

Figure 7 contrasts the anisotropy decay of water in the $w_0 = 5$ and $w_0 = 10$ reverse micelles at 2558 cm^{-1}. The $w_0 = 10$ data have a larger amplitude and slower initial decay and reach a plateau at longer times, whereas the $w_0 = 5$ signal continues to decay. It is counterintuitive for the larger reverse micelle with a smaller fraction of water in contact with the interface to have a slower long-time reorientation. On the basis of geometric considerations, it was found that 64% of the water molecules in the $w_0 = 10$ reverse micelles do not directly interact with the interface but that, in the $w_0 = 5$ reverse micelles, nearly all the water molecules interact with the interface. The initial decay of the water in $w_0 = 10$ data is substantially slower than the early-time wobbling-in-a-cone portion of the water in $w_0 = 5$ data.

These data indicate the presence of more than one water ensemble in the $w_0 = 10$ reverse micelle with distinct vibrational lifetimes and orientational correlation times. The question is whether the $w_0 = 10$ reverse micelle contains enough water to allow it to adopt the bulk-like characteristics observed in large reverse micelles. The plateau behavior at longer times in $w_0 = 10$ reverse micelles resembles that observed for $w_0 = 25$ (see **Figure 5**) and other large reverse micelles. For large reverse micelles, with the exceptions of size and the wavelength-dependent fraction a, we know all of the parameters: Water in the core has a 1.8-ps lifetime and a 2.6-ps orientational relaxation time, and the interfacial water has a 4.3-ps lifetime and an 18-ps orientational relaxation time. If the $w_0 = 10$ water nanopool has a bulk-like core and the same interface dynamics as the larger reverse micelles, then we should be able to adjust a to obtain a good fit of

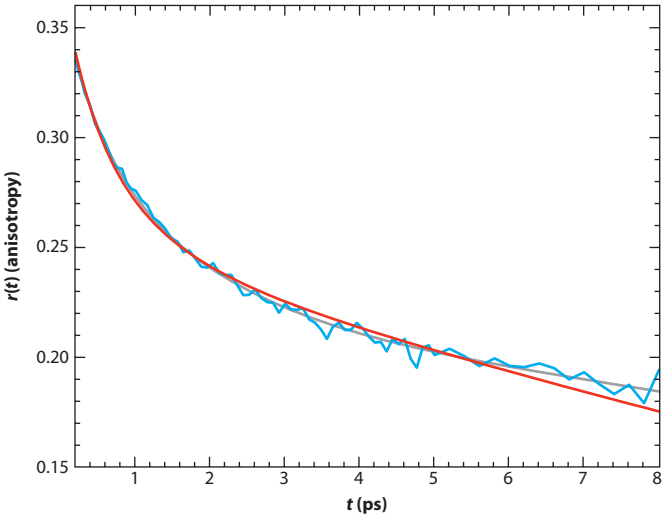

Figure 8

Anisotropy decay for water (5% HOD in H_2O) in $w_0 = 10$ (*blue line*) with fits to two different models. The red curve represents a fit to Equation 6; only *a* varies, and $T_1^w = 1.8$ ps, $T_1^i = 4.3$ ps, $\tau_r^w = 2.6$ ps, and $\tau_r^i = 18$ ps (parameters for large reverse micelles) (9). The gray line represents global fits to Equations 5 and 6 for vibrational relaxation and anisotropy decays, yielding a core lifetime of $T_{\text{core}} = 2.2$ ps, a core orientational correlation time of $\tau_{\text{core}} = 4.0$ ps, an interfacial vibrational lifetime of $T_{\text{int}} = 5.3$ ps, and an interfacial orientational correlation time of $\tau_{\text{int}} = 26$ ps.

the data. **Figure 8** displays the $w_0 = 10$ anisotropy data and two different fits. The fit does not capture the shape of the anisotropy decay via the large reverse micelle time constants. The fit is systematically too high in the middle of the data, and it is too low and decays too fast at longer times.

The failure of the large reverse micelle parameters to reproduce the $w_0 = 10$ data indicates that the water in these environments is intermediate between the completely coupled situation in small reverse micelles and the strict two-component model for large reverse micelles. The impact of the interface slows water–hydrogen bond dynamics and also influences the water dynamics away from the interface, but unlike in very small reverse micelles, the water molecules do not behave as a single ensemble. Also, the vibrational lifetime of the water away from the interface may differ from that of bulk water due to perturbations in the hydrogen bonding network. To account for the intermediate behavior, we used Equations 5 and 6, allowing the vibrational lifetime and orientational correlation time of both the core and interfacial water to vary, but requiring values to be longer than the bulk water and large reverse micelle interfacial values. To gain confidence in this model, which has so many adjustable parameters, lifetimes were fit independently from the orientational relaxation times in a manner similar to that shown in **Figure 4**. Also, data from a range of frequencies were fit globally to the same parameters, except for the fraction of core water, *a*. The result is shown in **Figure 8** as a two-component fit to the $w_0 = 10$ anisotropy decays and vibrational population relaxations for a range of frequencies. The resulting fit is quite good. The water dynamics are slower in both regions than in large reverse micelles, but two distinct types of water molecules still exist in the $w_0 = 10$ reverse micelle, unlike in small reverse micelles.

Two important factors can contribute to the transition from two-component dynamics to collective dynamics. The first is related to the mechanism of water reorientation (discussed briefly above). Laage & Hynes (3, 4) showed that water reorientation occurs through a transition state that

involves a bifurcated hydrogen bond formed between the old and new hydrogen bond acceptors by the water molecule under observation. The new acceptor, originally in the second hydration shell of the rotating water molecule, moves through concerted motions into the first hydration shell, creating an overcoordinated environment for the rotating water molecule and reducing the energetic barrier for reorientation. This model shows that water reorientation is not a localized process: The reorientation of a single water molecule requires concerted rearrangement of both its first and its second hydration shell, involving ~16 water molecules (61). If 1 or more of these 16 water molecules is itself in an environment different from bulk water, causing it to have dynamics distinct from those of bulk water, it affects the dynamics of its neighbors. In the presence of many unperturbed water molecules, such as in large reverse micelles, the effect of the perturbation decays away relatively quickly. However, in intermediate reverse micelles, so many of the water molecules are perturbed that even water molecules not directly interacting with the interface have slower dynamics.

The second important factor is the changing structure of the reverse micelle interface, which occurs as the reverse micelle size decreases. In large reverse micelles, the curvature of the interface is relatively gentle, presenting a nearly planar surface to the water pool. The nature of the interface changes relatively gradually between $w_0 = 46$ and $w_0 = 16.5$, but below $w_0 = 16.5$ important structural changes occur at the interface that contribute to the transition from two-component to collective dynamics. Both MD simulations (47) and IR spectroscopy of the head group moieties of AOT (62–64) show that there is increased association between the sulfonate head groups and sodium counterions at lower hydration levels. This association leads to a rigid structure of ionic interactions wherein water molecules are trapped between sodium ions and sulfonate head groups. At $w_0 = 10$ there is a small amount of ion pairing, but the effects become increasingly important below $w_0 = 6$ (62). Also, the surface area per AOT decreases dramatically below $w_0 = 10$ (46). Very small reverse micelles have low surface area per AOT and significant surface curvature, allowing water molecules to interact with multiple sulfonate groups simultaneously, which in turn increases the degree of perturbation. The change in surface area occurs fairly rapidly as the reverse micelle size increases, and by $w_0 = 16.5$ it has almost reached its limiting value. The similarities among the surface areas per head group may explain why all the reverse micelles with $w_0 \geq 16.5$ have the same interfacial dynamics. Essentially, for large reverse micelles the nature of the interface is independent of reverse micelle size.

6. CONCLUDING REMARKS

Large AOT reverse micelles ($w_0 \geq 16.5$, $d \geq 5.5$ nm) possess two water ensembles: One comprises the core, which is well removed from the interface, and the other includes water at the interface. The core water has bulk properties, and water in the core undergoes orientational relaxation with the same decay time (2.6 ps) as bulk water. Water at the interface undergoes much slower orientational relaxation, with a decay time of 18 ps. For large reverse micelles, the interfacial orientational relaxation time, and therefore the hydrogen bond dynamics, is independent of the size of the water nanopool.

In small reverse micelles ($w_0 \leq 5$, $d \leq 2.5$ nm), experiments indicate essentially a single water ensemble, within experimental error, with no distinct core. All of the water molecules are strongly influenced by their proximity to the interface. The orientational relaxation time depends heavily on size and increases substantially as the size of the water nanopool decreases. For $w_0 = 5$ ($d = 2.5$ nm), the orientational relaxation time is 30 ps. For $w_0 = 2$ ($d = 1.7$ nm), the orientational relaxation time is 110 ps. The experiments find no wavelength dependence for the orientational dynamics within experimental error, which indicates a single ensemble. However, recent MD

simulations show some variation in the dynamics of water, depending on the position within the small number of water molecules (47).

Intermediate-size reverse micelles ($5 \leq w_0 \leq 16.5$, $2.5 \leq d \leq 5.5$ nm) also display two water ensembles. However, the core does not consist of bulk-like water. The reverse micelles in the intermediate range are small enough that the influence of the interface affects all of the water in the nanopool but not to a large enough extent to produce a single ensemble. For $w_0 = 10$, the core water and the interfacial water have orientational relaxation times of 4 ps and 26 ps, respectively, which are slower than the relaxation times of large reverse micelles.

The work presented here describes water dynamics in AOT spherical reverse micelles. A recent study compared water dynamics at the interface of AOT lamellar structures, which have slabs of water that are infinite in two dimensions but are confined by planar interfaces (9). The orientational relaxation in the lamellae is the same as in the large AOT reverse micelles. Reverse micelles and lamellae with the same number of waters per head group behave the same as one another, rather than as reverse micelles with diameters equal to the interplanar spacing of the lamellae. Therefore, once the spheres are sufficiently large, the geometry of the confining structure (spherical or planar) is no longer crucial. Another study compared the same large-size ($d = 9$ nm) AOT and Igepal® CO-520 reverse micelles. AOT has an ionic head group, whereas Igepal is neutral. The Igepal data are described well by a bulk-like water core and interfacial water. The orientational relaxation at the nonionic Igepal interface is slightly faster (13 ps) than that for AOT (18 ps), but the error bars overlap somewhat. We conclude that the presence of the interface, rather than the chemical nature of the interface, plays the dominant role in controlling interfacial hydrogen bond dynamics.

The work presented here provides insights into the nature of water dynamics in a variety of other systems, such as cell membranes (65–68), the surfaces of proteins (69), channels in polyelectrolyte fuel cell membranes (59, 70), and many others. Confinement and interfaces affect water dynamics and thus processes that take place in water, for example, electronic excited-state solvation (71–74) and proton transfer (75–79). Studies such as those presented above, as well as increasingly sophisticated simulations of water in confinement, are greatly increasing our understanding of water and of the processes that occur in nanoconfined systems.

DISCLOSURE STATEMENT

The authors are not aware of any affiliations, memberships, funding, or financial holdings that might be perceived as affecting the objectivity of this review.

ACKNOWLEDGMENTS

M.D.F. thanks the U.S. Department of Energy (DE-FG03-84ER13251), the National Institutes of Health (2-R01-GM061137-09), and the National Science Foundation (DMR 0652232) for support of this work. N.E.L. thanks the National Science Foundation (CHE 0649263) for support of this work. In addition, we thank Ruth E. Riter, David E. Moilanen, Emily E. Fenn, Daryl Wong, and Ivan R. Piletic, who made major contributions to the work discussed here.

LITERATURE CITED

1. Steinel T, Asbury JB, Zheng J, Fayer MD. 2004. Watching hydrogen bonds break: a transient absorption study of water. *J. Phys. Chem. A* 108:10957–64

2. Bertie J, Lan Z. 1996. Infrared intensities of liquids. 20. The intensity of the OH stretching band of liquid water revisited, and the best current values of the optical constants of H_2O(1) at 25 degrees C between 15,000 and 1 cm^{-1}. *Appl. Spectrosc.* 50:1047–57
3. Laage D, Hynes JT. 2006. A molecular jump mechanism of water reorientation. *Science* 311:832–35
4. Laage D, Hynes JT. 2008. On the molecular mechanism of water reorientation. *J. Phys. Chem. B* 112:14230–42
5. Laage D, Hynes JT. 2008. On the residence time for water in a solute hydration shell: application to aqueous halide solutions. *J. Phys. Chem. B* 112:7697–701
6. Moilanen DE, Fenn EE, Lin Y-S, Skinner JL, Bagchi B, Fayer MD. 2008. Water inertial reorientation: hydrogen bond strength and the angular potential. *Proc. Natl. Acad. Sci. USA* 105:5295–300
7. Qvist J, Halle B. 2008. Thermal signature of hydrophobic hydration dynamics. *J. Am. Chem. Soc.* 130:10345–53
8. Laage D, Stirnemann G, Hynes JT. 2009. Why water reorientation slows without iceberg formation around hydrophobic solutes. *J. Phys. Chem. B* 113:2428–35
9. Moilanen DE, Fenn EE, Wong DB, Fayer MD. 2009. Water dynamics in large and small reverse micelles: from two ensembles to collective behavior. *J. Chem. Phys.* 131:014704
10. Petersen C, Tielrooij KJ, Bakker HJ. 2009. Strong temperature dependence of water reorientation in hydrophobic hydration shells. *J. Chem. Phys.* 130:214511
11. Rey R, Ingrosso F, Elsaesser T, Hynes JT. 2009. Pathways for H_2O bend vibrational relaxation in liquid water. *J. Phys. Chem. A* 113:8949–62
12. Sovago M, Campen RK, Bakker HJ, Bonn M. 2009. Hydrogen bonding strength of interfacial water determined with surface sum-frequency generation. *Chem. Phys. Lett.* 470:7–12
13. Tielrooij KJ, Petersen C, Rezus YLA, Bakker HJ. 2009. Reorientation of HDO in liquid H_2O at different temperatures: comparison of first and second order correlation functions. *Chem. Phys. Lett.* 471:71–74
14. Timmer RLA, Bakker HJ. 2009. Hydrogen bond fluctuations of the hydration shell of the bromide anion. *J. Phys. Chem. A* 113:6104–10
15. Hamm P, Lim M, Hochstrasser RM. 1998. Non-Markovian dynamics of the vibrations of ions in water from femtosecond infrared three-pulse photon echoes. *Phys. Rev. Lett.* 81:5326
16. Stenger J, Madsen D, Hamm P, Nibbering ETJ, Elsaesser T. 2002. A photon echo peak shift study of liquid water. *J. Phys. Chem. A* 106:2341–50
17. Fecko CJ, Eaves JD, Loparo JJ, Tokmakoff A, Geissler PL. 2003. Ultrafast hydrogen-bond dynamics in the infrared spectroscopy of water. *Science* 301:1698–702
18. Asbury JB, Steinel T, Kwak K, Corcelli S, Lawrence CP, et al. 2004. Dynamics of water probed with vibrational echo correlation spectroscopy. *J. Chem. Phys.* 121:12431–46
19. Asbury JB, Steinel T, Stromberg C, Corcelli SA, Lawrence CP, et al. 2004. Water dynamics: vibrational echo correlation spectroscopy and comparison to molecular dynamics simulations. *J. Phys. Chem. A* 108:1107–19
20. Heyne K, Nibbering ETJ, Elsaesser T, Petkovic M, Kuhn O. 2004. Cascaded energy redistribution upon O-H stretching excitation in an intramolecular hydrogen bond. *J. Phys. Chem. A* 108:6083–86
21. Fecko CJ, Loparo JJ, Roberts ST, Tokmakoff A. 2005. Local hydrogen bonding dynamics and collective reorganization in water: ultrafast infrared spectroscopy of HOD/D_2O. *J. Chem. Phys.* 122:054506
22. Loparo JJ, Roberts ST, Tokmakoff A. 2006. Multidimensional infrared spectroscopy of water. I. Vibrational dynamics in two-dimensional IR line shapes. *J. Chem. Phys.* 125:194521
23. Loparo JJ, Roberts ST, Tokmakoff A. 2006. Multidimensional infrared spectroscopy of water. II. Hydrogen bond switching dynamics. *J. Chem. Phys.* 125:194522
24. Moilanen DE, Wong DB, Rosenfeld DE, Fenn EE, Fayer MD. 2009. Ion-water hydrogen bond switching observed with 2D IR vibrational echo chemical exchange spectroscopy. *Proc. Natl. Acad. Sci. USA* 106:375–80
25. Auer B, Kumar R, Schmidt JR, Skinner JL. 2007. Multidimensional ultrafast spectroscopy special feature: hydrogen bonding and Raman, IR, and 2D-IR spectroscopy of dilute HOD in liquid D_2O. *Proc. Natl. Acad. Sci. USA* 104:14215–20

4. Presents details of a jump-reorientation model for water reorientation in which a bifurcated hydrogen bond must form for reorientation to occur.

8. Theoretical model explains that slowed dynamics for water reorientation near a hydrophobic solute arise because the hydrogen atom lacks nearby water in which to switch its hydrogen bond.

9. Demonstrates that water dynamics in confinement arise from ensembles of molecules at the interface and in the core of reverse micelles.

26. Mallik BS, Semparithi A, Chandra A. 2008. Vibrational spectral diffusion and hydrogen bond dynamics in heavy water from first principles. *J. Phys. Chem. A* 112:5104–12
27. Falvo C, Palmieri B, Mukamel S. 2009. Coherent infrared multidimensional spectra of the OH stretching band in liquid water simulated by direct nonlinear exciton propagation. *J. Chem. Phys.* 130:184501
28. Skinner JL, Auer BM, Lin YS. 2009. Vibrational line shapes, spectral diffusion, and hydrogen bonding in liquid water. In *Advances in Chemical Physics*, ed. SA Rice, 142:59–103. New York: Wiley
29. Bakker HJ, Woutersen S, Nienhuys HK. 2000. Reorientational motion and hydrogen-bond stretching dynamics in liquid water. *Chem. Phys.* 258:233–45
30. Nienhuys H-K, van Santen RA, Bakker HJ. 2000. Orientational relaxation of liquid water molecules as an activated process. *J. Chem. Phys.* 112:8487–94
31. Loparo JJ, Fecko CJ, Eaves JD, Roberts ST, Tokmakoff A. 2004. Reorientational and configurational fluctuations in water observed on molecular length scales. *Phys. Rev. B* 70:180201
32. Rezus YLA, Bakker HJ. 2005. On the orientational relaxation of HDO in liquid water. *J. Chem. Phys.* 123:114502
33. Bakker HJ, Rezus YLA, Timmer RLA. 2008. Molecular reorientation of liquid water studied with femtosecond midinfrared spectroscopy. *J. Phys. Chem. A* 112:11523–34
34. Møller KB, Rey R, Hynes JT. 2004. Hydrogen bond dynamics in water and ultrafast infrared spectroscopy: a theoretical study. *J. Phys. Chem. A* 108:1275–89
35. Loparo JJ, Roberts ST, Nicodemus RA, Tokmakoff A. 2007. Variation of the transition dipole moment across the OH stretching band of water. *Chem. Phys.* 341:218–29
36. Cowan ML, Bruner BD, Huse N, Dwyer JR, Chugh B, et al. 2005. Ultrafast memory loss and energy redistribution in the hydrogen bond network of liquid H_2O. *Nature* 434:199–202
37. Huse N, Bruner BD, Cowan ML, Dreyer J, Nibbering ETJ, et al. 2005. Anharmonic couplings underlying the ultrafast vibrational dynamics of hydrogen bonds in liquids. *Phys. Rev. Lett.* 95:147402
38. Dokter AM, Woutersen S, Bakker HJ. 2005. Anomalous slowing down of the vibrational relaxation of liquid water upon nanoscale confinement. *Phys. Rev. Lett.* 94:178301
39. Gilijamse JJ, Lock AJ, Bakker HJ. 2005. Dynamics of confined water molecules. *Proc. Natl. Acad. Sci. USA* 102:3202–7
40. Tan H-S, Piletic IR, Riter RE, Levinger NE, Fayer MD. 2005. Dynamics of water confined on a nanometer length scale in reverse micelles: ultrafast infrared vibrational echo spectroscopy. *Phys. Rev. Lett.* 94:057405
41. Dokter AM, Woutersen S, Bakker HJ. 2006. Inhomogeneous dynamics in confined water nanodroplets. *Proc. Natl. Acad. Sci. USA* 103:15355–58
42. Piletic I, Tan H-S, Moilanen DE, Spry DB, Fayer MD. 2006. Vibrational echo and pump-probe spectroscopic studies of the dynamics of water molecules confined to nanoscopic dimensions. In *Femtochemistry VII: Fundamental Ultrafast Processes in Chemistry, Physics, and Biology*, ed. AW Castleman, ML Kimble, pp. 195–203. Amsterdam: Elsevier
43. Piletic IR, Moilanen DE, Spry DB, Levinger NE, Fayer MD. 2006. Testing the core/shell model of nanoconfined water in reverse micelles using linear and nonlinear IR spectroscopy. *J. Phys. Chem. A* 110:4985–99
44. Dokter AM, Woutersen S, Bakker HJ. 2007. Ultrafast dynamics of water in cationic micelles. *J. Chem. Phys.* 126:124507
45. Moilanen DE, Levinger N, Spry DB, Fayer MD. 2007. Confinement or properties of the interface? Dynamics of nanoscopic water in reverse micelles. *J. Am. Chem. Soc.* 129:14311–18
46. De TK, Maitra A. 1995. Solution behavior of Aerosol OT in nonpolar solvents. *Adv. Colloid Interface Sci.* 59:95–193
47. Faeder J, Ladanyi BM. 2000. Molecular dynamics simulations of the interior of aqueous reverse micelles. *J. Phys. Chem. B* 104:1033–46
48. Zulauf M, Eicke H-F. 1979. Inverted micelles and microemulsions in the ternary system water/Aerosol-OT/isooctane as studied by photon correlation spectroscopy. *J. Phys. Chem.* 83:480–86
49. Kinugasa T, Kondo A, Nishimura S, Miyauchi Y, Nishii Y, et al. 2002. Estimation for size of reverse micelles formed by AOT and SDEHP based on viscosity measurement. *Colloid Surf. A* 204:193–99
50. Piletic IR, Moilanen DE, Levinger NE, Fayer MD. 2006. What nonlinear-IR experiments can tell you about water that the IR spectrum cannot. *J. Am. Chem. Soc.* 128:10366–67

43. Presents a core-shell model for water confined inside reverse micelles and applies the model to steady-state infrared spectra, vibrational lifetimes, time-resolved anisotropy, and vibrational echo measurements.

51. Fenn EE, Wong DB, Fayer MD. 2009. Water dynamics at neutral and ionic interfaces. *Proc. Natl. Acad. Sci. USA* 106:15243–48

52. Moilanen DE, Fenn EE, Wong DB, Fayer MD. 2009. Geometry and nanolength scales vs. interface interactions: water dynamics in AOT lamellar structures and reverse micelles. *J. Am. Chem. Soc.* 131:8318–28

53. Moilanen DE, Fenn EE, Wong DB, Fayer MD. 2009. Water dynamics at the interface in AOT reverse micelles. *J. Phys. Chem. B* 113:8560–68

54. Piletic IR, Tan H-S, Fayer MD. 2005. Dynamics of nanoscopic water: vibrational echo and infrared pump-probe studies of reverse micelles. *J. Phys. Chem. B* 109:21273–84

55. Woutersen S, Bakker HJ. 1999. Resonant intermolecular transfer of vibrational energy in liquid water. *Nature* 402:507–9

56. Gaffney KJ, Piletic IR, Fayer MD. 2003. Orientational relaxation and vibrational excitation transfer in methanol–carbon tetrachloride solutions. *J. Chem. Phys.* 118:2270–78

57. Tokmakoff A. 1996. Orientational correlation functions and polarization selectivity for nonlinear spectroscopy of isotropic media. I. Third order. *J. Chem. Phys.* 105:1–12

58. Tan H-S, Piletic IR, Fayer MD. 2005. Orientational dynamics of nanoscopic water in reverse micelles: ultrafast infrared frequency selective transient absorption experiments. *J. Chem. Phys.* 122:174501

59. Moilanen DE, Piletic IR, Fayer MD. 2006. Tracking water's response to structural changes in Nafion membranes. *J. Phys. Chem. A* 110:9084–88

60. Fenn EE, Moilanen DE, Levinger NE, Fayer MD. 2009. Water dynamics and interactions in water-polyether binary mixtures. *J. Am. Chem. Soc.* 131:5530–39

61. Stanley HE, Kumar P, Xu L, Yan Z, Mazza MG, et al. 2007. The puzzling unsolved mysteries of liquid water: some recent progress. *Physica A* 386:729–43

62. Christopher DJ, Yarwood J, Belton PS, Hills BP. 1992. A Fourier transform IR study of water–head group interactions in reversed micelles containing sodium bis(2-ethylhexyl)sulfosuccinate (AOT). *J. Colloid Interface Sci.* 152:465–72

63. Moran PD, Bowmaker GA, Cooney RP, Bartlett JR, Woolfrey JL. 1995. Vibrational spectroscopic study of the structure of sodium bis(2-ethylhexyl)sulfosuccinate reverse micelles and water-in-oil microemulsions. *Langmuir* 11:738–43

64. Moran PD, Bowmaker GA, Cooney RP, Bartlett JR, Woolfrey JL. 1995. Vibrational-spectra of metal-salts of bis(2-ethylhexyl)sulfosuccinate (AOT). *J. Mater. Chem.* 5:295–302

65. Borgnia M, Nielsen S, Engel A, Agre P. 1999. Cellular and molecular biology of the aquaporin water channels. *Annu. Rev. Biochem.* 68:425–58

66. de Groot BL, Grubmuller H. 2001. Water permeation across biological membranes: mechanism and dynamics of aquaporin-1 and GlpF. *Science* 294:2353–57

67. Kandt C, Schlitter J, Gerwert K. 2004. Dynamics of water molecules in the bacteriorhodopsin trimer in explicit lipid/water environment. *Biophys. J.* 86:705–17

68. Volkov V, Hamm P. 2004. A two-dimensional infrared study of localization, structure, and dynamics of a dipeptide in membrane environment. *Biophys. J.* 87:4213–25

69. Pal SK, Peon J, Zewail AH. 2002. Biological water at the protein surface: dynamical solvation probed directly with femtosecond resolution. *Proc. Natl. Acad. Sci. USA* 99:1763–68

70. Moilanen DE, Piletic IR, Fayer MD. 2007. Water dynamics in Nafion fuel cell membranes: the effects of confinement and structural changes on the hydrogen bond network. *J. Phys. Chem. C* 111:8884–91

71. Sarkar N, Das K, Datta A, Das S, Bhattacharyya K. 1996. Solvation dynamics of coumarin 480 in reverse micelles. Slow relaxation of water molecules. *J. Phys. Chem.* 100:10523–27

72. Riter RE, Willard DM, Levinger NE. 1998. Water immobilization at surfactant interfaces in reverse micelles. *J. Phys. Chem. B* 102:2705–14

73. Willard DM, Riter RE, Levinger NE. 1998. Dynamics of polar solvation in lecithin/water/cyclohexane reverse micelles. *J. Am. Chem. Soc.* 120:4151–60

74. Bhattacharyya K, Bagchi B. 2000. Slow dynamics of constrained water in complex geometries. *J. Phys. Chem. A* 104:10603–13

75. Bhattacharyya K. 2003. Solvation dynamics and proton transfer in supramolecular assemblies. *Acc. Chem. Res.* 36:95–101

52. Reveals that the dynamics of water do not depend on the geometry of the interface.

53. Measures orientational dynamics of water in reverse micelles and determines contributions from bulk water in the reverse micellar core and interfacial water molecules at the inner surface.

76. Mohammed OF, Pines D, Dreyer J, Pines E, Nibbering ETJ. 2005. Sequential proton transfer through water bridges in acid-base reactions. *Science* 310:83–86
77. Mohammed OF, Pines D, Nibbering ETJ, Pines E. 2007. Base-induced solvent switches in acid-base reactions. *Angew. Chem. Int. Ed.* 46:1458–61
78. Mohammed OF, Pines D, Pines E, Nibbering ETJ. 2007. Aqueous bimolecular proton transfer in acid-base neutralization. *Chem. Phys.* 341:240–57
79. Spry DB, Goun A, Glusac K, Moilanen DE, Fayer MD. 2007. Proton transport and the water environment in Nafion fuel cell membranes and AOT reverse micelles. *J. Am. Chem. Soc.* 129:8122–30

Annual Review of
Analytical Chemistry

Volume 3, 2010

Contents

Indexes

Errata

An online log of corrections to *Annual Review of Analytical Chemistry* articles may be found at http://arjournals.annualreviews.org/errata/anchem.